Journal of Mining and Environment (JME) Vol. 17, No. 5, 2026, 1737-1751

Shahrood University of Technology

Journal of Mining and Environment (JME)

Journal homepage: www.jme.shahroodut.ac.ir

Iranian Society of Mining Engineering (IRSME)

An Instrumented Direct Tensile Testing Framework for Layered Materials: Experimental Validation and 3D PFC Analysis of Asymmetric Fracture

Vahab Sarfarazi[1], Hadi Haeri[2*], Pejman Kalvandi[1], Alireza Shaker[3], Mohammad Fatehi Marji[4], and Gholamreza Saeedi[5]

1.Department of Mining Engineering, Hamedan University of Technology, Hamedan, Iran.
2.Department of Mining Engineering, Higher Education Complex of Zarand, Shahid Bahonar University of Kerman, Kerman, Iran
3.Department of Geology, Faculty of Sciences, Shahid Bahonar University of Kerman, Kerman, Iran
4.Department of Mine Exploitation Engineering, Faculty of Mining and Metallurgy, Institute of Engineering, Yazd University, Yazd, Iran.
5.Department of Mining Engineering, Shahid Bahonar University of Kerman, Kerman, Iran

Article Info

Received 16 February 2026
Received in Revised form 30 May 2026
Accepted 4 August 2026
Published online 4 August 2026

DOI: 10.22044/jme.2026.17499.3478

Keywords

3D anisotropy models
Direct tensile strength
Crack initiation
Pre-holed layered sample

Abstract

Determining the tensile strength of brittle, layered materials, including layered rocks and cracked concrete, is difficult when using commonly adopted indirect loading configurations that do not induce pure tensile conditions. Therefore, obtaining tensile strength through direct experimental quantification is crucial for such materials, particularly when examining crack onset and subsequent crack growth in the vicinity of crack tips. The present research proposes a novel direct tension-based testing framework designed to deliver more reliable strength characterization of layered quasi-brittle materials, while simultaneously enabling a detailed assessment of fracture initiation and propagation mechanisms. The testing apparatus consists of a steel beam with a load converter that serves as both the loading fixture and the load cell. A pre-holed layered sample is securely positioned at the centre of the apparatus using a strong metal plate, while strain gauges on both sides capture critical data on the specimen's tensile behaviour. Significantly, the apparatus can detect and quantify asymmetric failure within the specimen, offering a detailed understanding of crack formation and failure patterns. The design, calibration protocols, and empirical test results are thoroughly detailed and analysed. Additionally, this study employs 3D PFC modelling to clarify the breakage mechanisms in various layer configurations, thereby enhancing the accuracy of tensile strength measurements. The numerical modelling results demonstrate that increasing the thickness of the hard layer leads to a nonlinear increase in the specimen's resistance. Furthermore, at a constant hard layer thickness, increasing the number of hard layers results in a decrease in the model's resistance.

1. Introduction

Anisotropy is a critical factor in various engineering fields and is particularly important in rock mechanics [1-5]. Many types of rock formations, including sedimentary rocks like shale, mudstone, and sandstone, as well as metamorphic rocks such as slate, gneiss, and schist, and even materials like coal and marl, exhibit mechanical anisotropy. This property influences the rocks' mechanical characteristics such as strength and elasticity depending on the direction of the applied force. Accurate evaluation of the strength properties of anisotropic rocks is vital since activities like tunneling, rock drilling, and slope excavation often involve these types of formations. Recognizing the presence of mechanical anisotropy is crucial during the design and analysis phases of rock engineering projects. Failing to account for this property can lead to significant errors in calculations and predictions regarding how the rock will respond to stress. The magnitude of these errors is directly related to the degree of anisotropy within the rock mass. Therefore, a

Corresponding author: hadihaeri@uk.ac.ir (H. Haeri)

comprehensive understanding and consideration of mechanical anisotropy are essential for reliable rock engineering assessments [1]. Sedimentary rocks, formed from deposited sediments, commonly exhibit lamination a parallel layering that greatly impacts their mechanical properties. This lamination, prevalent in rocks like shale, sandstone, and limestone, significantly affects their directional anisotropy. It is crucial to understand how lamination influences the directional load dependence of material properties in laminated rocks, as this knowledge is vital for planning and executing infrastructure projects. Addressing these factors ensures long-term safety and promotes the efficient design of structures built on or within laminated sedimentary rock formations [4]. To accurately determine the geotechnical properties of laminated and anisotropic rock formations, various laboratory testing methods are employed. Common testing procedures include uniaxial compression tests, which apply a single axial force, and triaxial compression tests, which apply confining pressures alongside the axial load to better simulate in-situ stress conditions. Additionally, simpler and informative tests, such as point load tests and punch tests, are often conducted to gain further insights into the rock's behavior, supplementing data from more complex tests. These results enable engineers to predict how the rock will respond to the stresses imposed by underground structures and to design appropriate support systems. Researchers have extensively explored the strength behavior and failure patterns of anisotropic rocks using various techniques [6-22]. Notable studies include Broch's measurement of strength anisotropy across 33 distinct rock types using point load index strength in both parallel and perpendicular orientations to lamination [23] and Al-Harthi's examination of how planar structures impact the anisotropy of Ranyah sandstone in Saudi Arabia [24]. These studies underscore the critical need to understand the effects of elastic anisotropy on tunnel wall displacements and the mechanical properties of rocks, including failure modes, strength, and residual strength. Despite significant progress, gaps remain in the comprehensive understanding of anisotropic rock behavior under various stress conditions. For instance, the influence of layer orientation on tensile strength and failure patterns in jointed rock masses has not been thoroughly examined. Tensile strength, a crucial parameter for assessing the load-bearing capacity of rocks, is significantly lower than compressive strength, highlighting the necessity for further investigation into the anisotropy of tensile behaviors in geotechnical engineering. This study employs Brazilian tensile strength tests and advanced acoustic emission analysis to investigate the anisotropic behaviors of layered gypsum-concrete and other rock types. The Brazilian splitting tensile test is a widely used and respected indirect technique for determining the tensile strength of brittle materials, particularly rocks and concrete. Its popularity is largely due to the simplicity of specimen preparation and ease of execution in laboratory settings. During this test, a disc-shaped specimen is subjected to a diametral compression force. This specific loading configuration allows researchers and engineers to deduce the material's tensile strength based on its behavior under compression. To ensure a thorough characterization of the geomechanical properties, especially in the context of anisotropic rock formations, a suite of complementary tests will also be performed. The planned testing program includes uniaxial compressive strength tests, which assess a material's resistance to compressive forces applied in a single direction. Moreover, triaxial compressive strength tests will evaluate the rock's strength under more complex stress states, where it is subjected to compressive forces in three mutually perpendicular directions. The investigation may also incorporate point load tests, which are relatively quick and easy to perform, providing an indication of tensile and compressive strengths. Additionally, punch tests will be conducted to further assess tensile properties and overall strength characteristics of the anisotropic rock. This research aims to enhance the current understanding of anisotropic behaviors in rock mechanics, facilitating the development of more accurate predictive models for engineering applications. A comprehensive analysis of the relationship between layer orientation and the strength characteristics of laminated sedimentary rock provides significant engineering benefits. This is particularly important for the design of stable rock slopes, tunnels, and foundations. Furthermore, the study will address the underlying mechanisms behind the anisotropy of fracture patterns observed in direct tensile tests, contributing to a broader understanding of fracture pattern anisotropy. The study will build upon existing literature, including works by Cho et al. [1], Li et al. [17], and Wang et al. [25], among others. It will integrate recent advancements in acoustic emission analysis and other experimental methodologies to provide a nuanced understanding of the anisotropic mechanical properties of rocks. Castro et al. [26] determined the tensile strength of sandstone using

direct tensile testing and found that increasing porosity leads to a reduction in tensile strength. Zhang et al. [27] investigated the effect of loading rate on the tensile strength of red sandstone using direct tensile testing and found that increasing the loading rate results in a decrease in tensile strength. Rabat et al. [28] studied the effect of water content on the tensile behavior of sandstone using direct tensile testing and found that increasing water content reduces the tensile strength of rock. Pérez-Rey et al. [29] investigated the scale effect on the tensile strength of granite using different testing methods and found that increasing specimen size leads to a decrease in tensile strength.

The Compressive-to-Tensile Load Transformer (CTLT) device is fundamentally designed to obtain the direct tensile strength of rock. Unlike conventional direct tensile testing methods, which suffer from significant challenges in specimen preparation and specimen attachment to the loading jaws, the CTLT approach enables a simplified and practical specimen preparation and loading procedure. Furthermore, in the Brazilian test, the load distribution on the failure plane is non-uniform, whereas the CTLT device applies load under the most ideal loading conditions, ensuring a uniform stress distribution across the failure plane.

By examining tensile and compressive strength anisotropy under various conditions, this research will contribute to the safe and efficient design of infrastructure in anisotropic rock formations. In conclusion, understanding the anisotropic properties of rocks is essential for various engineering applications. This study seeks to address existing research gaps by employing a combination of traditional and advanced testing methods, providing a comprehensive understanding of anisotropic behaviors in rock mechanics. The insights gained from this research will be invaluable for the design and stability analysis of structures in sedimentary rock formations, ultimately contributing to the advancement of geotechnical engineering. It is worth noting that in this study, two distinct testing approaches were employed for different purposes. The Brazilian test was used exclusively for material calibration, enabling the determination of the tensile strength of the intact rock material applied in the numerical models. In contrast, the direct tensile test, conducted using the Compressive-to-Tensile Load Transformer (CTLT) device, was utilized solely for testing layered specimens.

2. Laboratory test

The pre-holed cylindrical samples, made up of alternating layers of gypsum and concrete, were carefully prepared for direct tensile testing to simulate sedimentary rock types. Concrete, which is known for its durability compared to gypsum, effectively mimics the high anisotropy ratios typically found in natural rock masses. In this study, gypsum was mixed with water in a 1.5:1 ratio. The cementation mixture consisted of fine sand, Portland cement, superplasticizer, tap water, and micro silica. The quantities for each material were as follows: 10,500 grams of sand, 2,800 grams of cement, 1,480 cc of water, 125 grams of superplasticizer, and 80 grams of micro silica. This combination enhances reproducibility and provides valuable insights into the tensile properties and failure mechanisms of stratified rocks. The aim of this setup is to improve the understanding of stress distribution and anisotropic characteristics within composite materials, leading to more accurate assessments and safer design practices in geotechnical engineering.

2.1. Mechanical characteristic of specimens

The mechanical properties of the specimens were evaluated through Brazilian and uniaxial compression tests. Laboratory experiments were carried out to characterize the material properties of Brazilian gypsum and concrete samples. Specifically, to determine the tensile strength of both concrete and mortar, the Brazilian standard method was employed. This involved using a disk with a radius of 27 mm and a thickness of 27 mm. The tests conducted to measure the indirect tensile strength yielded results of 0.65 MPa for the gypsum sample and 1.35 MPa for the concrete sample.

Further experiments were conducted to assess the compressive strength of both materials. Uniaxial compression tests were performed on rectangular prism specimens with dimensions of 300 mm in length, 160 mm in width, and 75 mm in thickness. The gypsum specimens demonstrated a compressive strength of 6 MPa when subjected to uniaxial compression. In contrast, the concrete specimens tested under the same conditions achieved a compressive strength of 18 MPa. These results reinforce the conclusion that concrete has significantly greater strength than gypsum in resisting both tensile and compressive forces.

2.2. Preparation of Samples with Layered Bedding

In this research project, the impact of concrete and gypsum bedding layers on the tensile failure mechanism of specimens was assessed using direct tensile testing. Samples with five distinct configurations of concrete and gypsum layers were meticulously prepared: three-layered specimens with either a gypsum or concrete interlayer, two-layered specimens with equal thicknesses of gypsum and concrete, two-layered specimens with the gypsum layer twice as thick as the concrete layer, and two-layered specimens with the concrete layer twice as thick as the gypsum layer (Figure 1). Each configuration was tested three times to ensure result accuracy. Large cylindrical plastic molds (150 × 60 mm) were utilized, with smaller cylindrical molds (50 × 60 mm) placed centrally (Figure 1a). These molds, constructed from rigid plastic, maintained dimensional stability during sample preparation. Before the casting process began, guidelines were marked on the interior surface of the molds, as shown in Figure 1b. These guidelines acted as visual aids for the subsequent pouring of materials. The primary casting materials used were gypsum and concrete. Once the molds were ready, gypsum and concrete were carefully poured into them. After pouring each material, the molds underwent a vibration process lasting 90 seconds to effectively eliminate any air pockets, ensuring a more solid and uniform final product. All specimens were cured at room temperature under ambient laboratory conditions until reaching sufficient strength before testing. To create samples with layered structures, a sequential pouring technique was employed. First, a layer of gypsum was poured into the mold and allowed to partially solidify. Once the gypsum had set enough, a layer of concrete was poured on top, carefully following the previously marked guidelines (Figure 1c). For three-layered samples, a final layer of gypsum was added on top after the initial gypsum and concrete layers were poured (Figure 1d). After the initial gypsum layer had hardened sufficiently, the mold removal process began. The inner mold (Figure 1e) was carefully detached and removed first, followed by the removal of the outer mold (Figure 1f). The specific layer percentages, indicating the proportions of concrete and gypsum used in each configuration of layered samples, are detailed in Table 1.

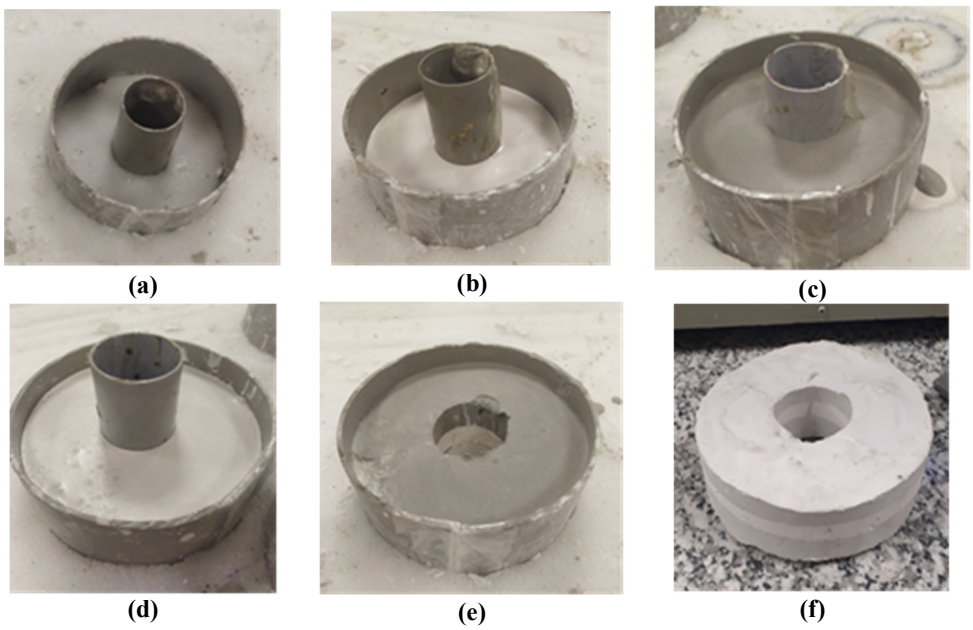

Figure 1. Illustration of the steps involved in preparing concrete-gypsum layered samples.

Table 2. Characteristics of the fabricated specimens, presenting the percentages of the concrete layer and gypsum layer for five different specimens.

	I	II	III	IV	VI
Concrete layer (%)	77	65	50	35	23
Gypsum layer (%)	23	35	50	65	77

2.3. A New Method for Measuring Direct Tension Tests Using Rectangular Geometries

The samples underwent direct tensile testing following a 28-day curing period to evaluate their strength and mechanical properties. This testing phase is crucial for understanding the material's behavior under tension, providing insights into its tensile strength, elasticity, and failure mechanisms. For each configuration, three identical specimens were prepared and tested. In cases where the data from one test was identified as an outlier, a fourth test was conducted to ensure the reliability and accuracy of the reported results. The average values along with the standard deviation for each configuration are reported in Table 1.

2.3.1. Apparatus for Direct Tensile Strength Testing

A specialized apparatus was engineered to evaluate the true tensile strength of cylindrical specimens. The system is composed of four principal elements manufactured from hardened stainless steel (Figure 2). The first component is formed by a pair of bracket-like elements with a Π-type geometry, whose lateral projections correspond to "I" and "L" shapes on the left and right sides, respectively (see Figure 2g). The second component is an integral block exhibiting a U-shaped profile (see Figure 2g) in the frontal view and a Π-type configuration in the lateral view, with its detailed geometry presented in Figure 2. The third component comprises two half-cylindrical steel collars, each having an outer diameter of 7.5 cm, a wall thickness of 1 cm, and an axial length of 6 cm. The fourth component comprises two steel blades, each measuring 19 cm in length, 1 cm in thickness, and 2 cm in width, as illustrated in Figure 2.

2.3.2. Loading Configuration

The direct tensile testing setup illustrated in Figure 2 was actuated by a 10-ton loading device, which applied compressive forces to induce tensile stresses within the specimen. Each tensile test lasted approximately 10 minutes, utilizing three specimens for accuracy. A loading rate of 0.02 MPa/s, endorsed by numerous researchers [33], was deemed optimal for material splitting tests.

Within the experimental framework of the direct tension setup, vertical tensile forces transmitted to the upper and lower portions of the specimen's central aperture induced the nucleation and propagation of two horizontal fissures at the point of failure. The mechanical load was transmitted by two slender steel blades, each 19 cm in length, 2 cm in width, and 1 cm in thickness. The contact area at the central aperture of the specimen was approximately 2 cm × 5 cm (Figure 2). To determine the tensile forces at the point of structural failure, referred to as Ft1 and Ft2, a calculation was performed. This involved taking the load that caused the material to fail, known as the failure load, and dividing it by a specific area. The area used for this calculation was not arbitrary; it was the failure surface area corresponding directly to the analyzed layer. As a result, the tensile forces at failure, Ft1 and Ft2, were calculated by dividing the experimentally measured breakage load by the respective failure surface area of each layer. This method of force application ensures precise measurement of tensile strength and failure behavior, providing critical data on the mechanical integrity of the layers. The observed horizontal cracks indicate a tensile failure mode, which is essential for understanding stress distribution and fracture mechanics. Quantifying Ft1 and Ft2 offers detailed insight into material performance under tensile stress, facilitating the development of predictive models and the optimization of material properties for enhanced durability and performance in practical applications.

$$F_{t1} = \left(\frac{t1}{t1 + t2} \times F\right) \tag{1}$$

$$F_{t2} = \left(\frac{t2}{t1 + t2} \times F\right) \tag{2}$$

In dual-layer samples, the externally applied forces Ft1 and Ft2 were partitioned across the respective layers. Thickness values t1 and t2 correspond to the gypsum and concrete layers, respectively. During the test, the maximum applied force F is measured at the point of failure. In this method, the tensile strength (σ_t) is determined through calculation by applying force proportionally to each layer relative to the corresponding fracture area.

$$\sigma_t = \left(\frac{F_{t1}}{b \times t1}\right) + \left(\frac{F_{t2}}{b \times t2}\right) \tag{3}$$

$$\sigma_t = \left(\frac{\frac{t1}{t1 + t2} \times F}{b \times t1}\right) + \left(\frac{\frac{t2}{t1 + t2} \times F}{b \times t2}\right) \tag{4}$$

The net diameter of the ring sample, b, was 10 cm, calculated as 15 cm minus 5 cm. The values of t1 and t2 for the tested specimens are determined

based on the proportions of mortar and concrete (Table 1) in each specimen.

2.4. laboratory results of the direct tensile tests

2.4.1. Breakage pattern

The breakage patterns observed in the experimental samples with varying thicknesses of concrete and gypsum layers are illustrated in Figure 3. In this figure, the white color represents the gypsum layer, while the dark grey color represents the concrete layer. In these samples, tensile cracks initially developed in the gypsum layers before propagating into the concrete layer.

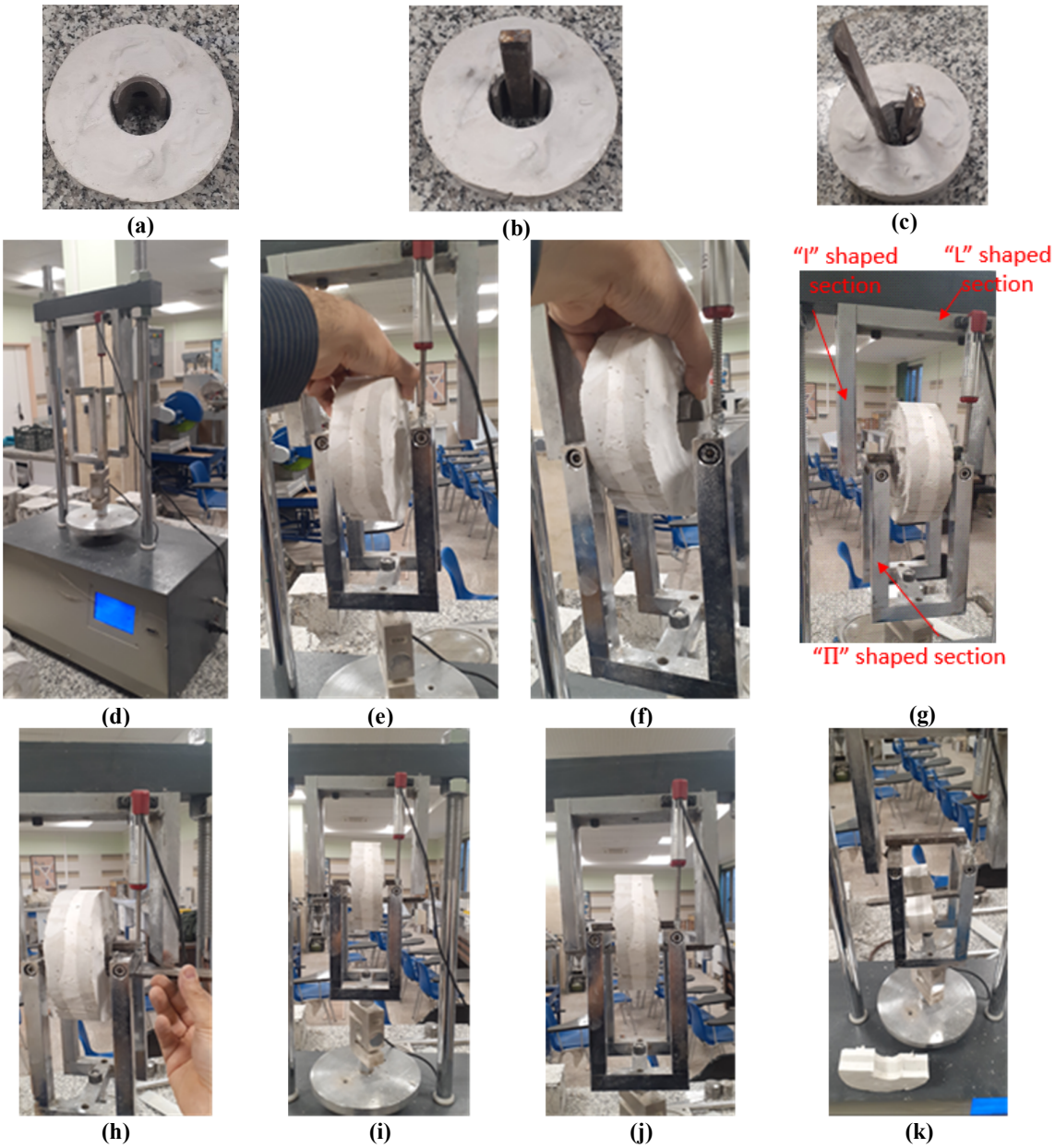

Figure 2. Disc sample with a central hole to measure the tensile strength directly by the tensile testing machine

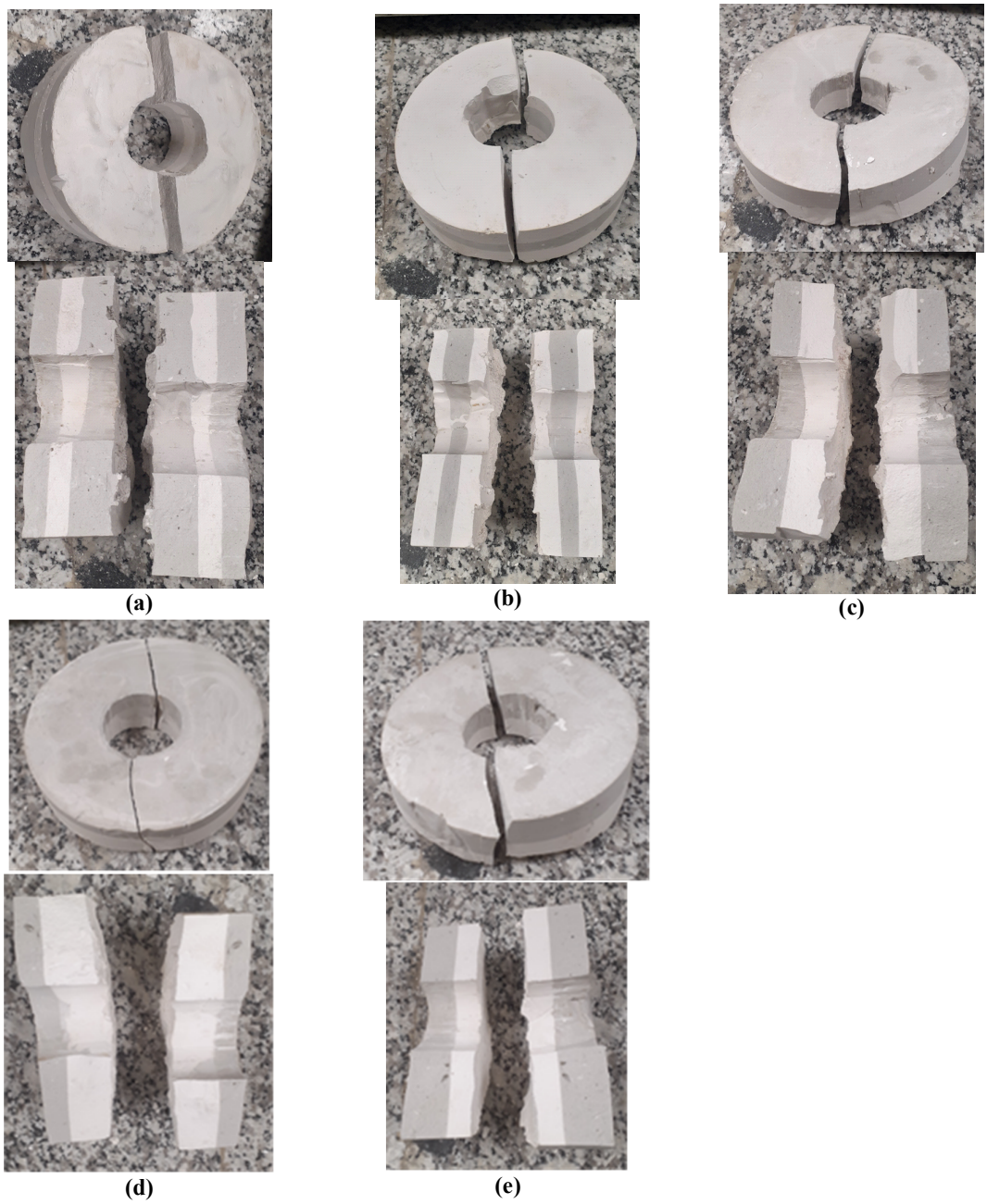

Figure 3. Failure pattern of layered pre-hold ring rock, a) three layered with gypsum middle layer, b) three layered with grout middle layer, c) two layers with same thickness, d) two layers with gypsum layer thickness of two times of grout layer, e) two layers with grout layer thickness of two times of gypsum layer.

2.4.2. Mechanical Behavior of Layered Concrete-Gypsum Samples

Figure 10 delineates the comprehensive stress-strain paradigms for stratified rock samples with varying proportions of constituent layers, offering a nuanced understanding of their tensile behavior. The stress-strain trajectories exhibit a pronounced linear elasticity culminating at the apex of tensile strength, succeeded by a precipitous decline. This data elucidates a direct correlation between the tensile strength and the percentage of the more resilient concrete layer, accentuating the material's anisotropic characteristics engendered by the interspersed, less robust gypsum layers. Notably, specimens with an augmented proportion of gypsum manifest diminished peak tensile strengths coupled with elevated critical strain values, signifying a delayed failure onset.

The observation that the critical strain escalates concomitantly with an increased percentage of the

gypsum layer implies that the deformation capacity prior to failure is substantially dictated by the softer material's presence. This interplay between the layers' mechanical properties suggests that the failure mechanisms are intricately linked to the heterogeneity of the material composition. The differential behavior under tensile loading underscores the necessity for a thorough comprehension of the material's composite nature, particularly for applications that demand rigorous performance predictability under tensile stresses. Such insights are pivotal for advancing the design and utilization of composite rock materials in engineering practices.

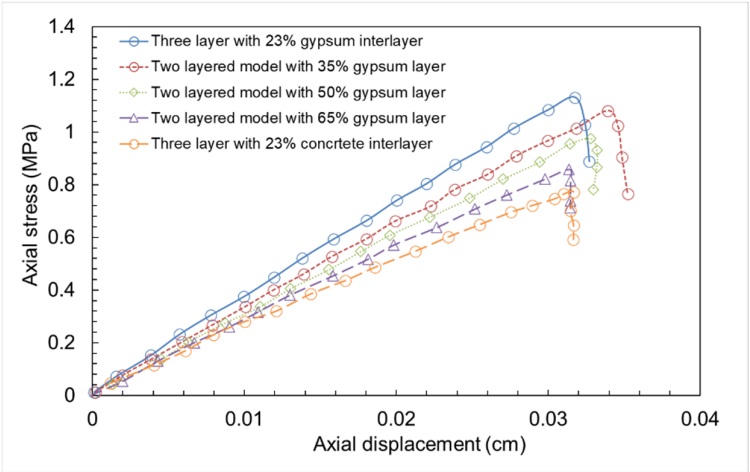

Figure 4. Representation of the mechanical behavior (stress-strain) for layered samples with different layering percentages.

3. Computational Simulation

3.1. PFC

A polygonal grain configuration of spheres was utilized by Potyondy [31] to create the flat joint (FJ) model, which consists of rigid spheres attached to flat notional surfaces. In the discrete element method (DEM) simulation of jointed geomaterial specimens, the flat joint model (FJM) is utilized. This model employs faceted grains depicted as lines in two dimensions or disks in three dimensions with domains. The FJM is implemented within a ball assembly, with a focus on the FJ contacts between the grains of the geomaterial. In this simulation, the grains are divided into bonded or unbonded elements, with FJs defined at the points where the grains come into contact. Initially, all forces and torques are set to zero, and these values are later modified according to bonding force-displacement laws and the relative movements of the faces. Shear forces are gradually adjusted, while normal forces are altered directly. The bonded elements in the modeled assembly exhibit linear behavior until they exceed their strength thresholds (σ(e) max and τ(e) max). Additionally, these elements provide significant rotational resistance with minimal applied torque in the simulation. Unbonded elements exhibit linear elasticity with frictional slip. FJ contacts endure damage upon bonded element rupture, and if displaced beyond their diameter and reestablish contact, the linear contact model is reinstated [31, 32].

The micro-mechanical parameters used in the PFC model include Young's modulus, normal-to-shear stiffness ratio, cohesion and its standard deviation, and tensile strength and its standard deviation. The macro-property calibration procedure was carried out through the following sequential steps. First, a uniaxial compressive test was simulated, and the micro-scale Young's modulus was adjusted iteratively until the macro-scale Young's modulus matched the experimentally measured value. Then, the normal-to-shear stiffness ratio was adjusted until the macro-scale Poisson's ratio was calibrated. Subsequently, the cohesion and tensile strength micro-parameters were modified until the macro-scale uniaxial compressive strength was calibrated. A Brazilian test was then simulated to determine the macro-scale tensile strength; if not adequately calibrated, the ratio of cohesion to tensile strength was adjusted iteratively until both compressive and tensile strengths were simultaneously calibrated. The standard deviations of cohesion and tensile strength were used to calibrate the crack initiation stress. Regarding the contact model, shear and tensile forces are applied at the bond interfaces and calculated using F = KU. These forces are divided

by the contact area to determine the interfacial stresses. When these stresses exceed the bond shear or tensile strength, the bond breaks, resulting in either a shear crack or a tensile crack. The shear strength of the bond follows the Mohr-Coulomb criterion, while the tensile strength is governed by the flat joint contact model. Prior to installing the flat joint contacts, floating particles were removed from the assembly and an isotropic stress was applied to ensure a stable initial condition. In this study, the flat joint contact model was employed as the bond between particles. This model has the capability to ideally approximate the ratio of compressive strength to tensile strength of rock, making it particularly suitable for simulating rock-like materials.

3.2. Calibration of PFC3D

To calibrate the micro-mechanical properties of intact concrete and gypsum, the trial-and-error method outlined by Abharian et al. [33] was employed. The stress-strain curves for both models are shown in Abharian et al. [33].

3.3. PFC Modelling of Layered Samples

Ring tests were conducted to numerically simulate the physical properties of interfaces between gypsum and concrete using a calibrated PFC3D model for the layered cylindrical structures (Figure 5). In this study, five samples with different layering configurations, including concrete and gypsum, were used to enhance the understanding of anisotropy and layering. As shown in Table 1, each sample consists of various proportions. The PFC3D sample had a diameter of 150 mm and included a 50 mm internal hole. It also incorporated micro-parameters for the simulated models of both the gypsum and concrete layers.

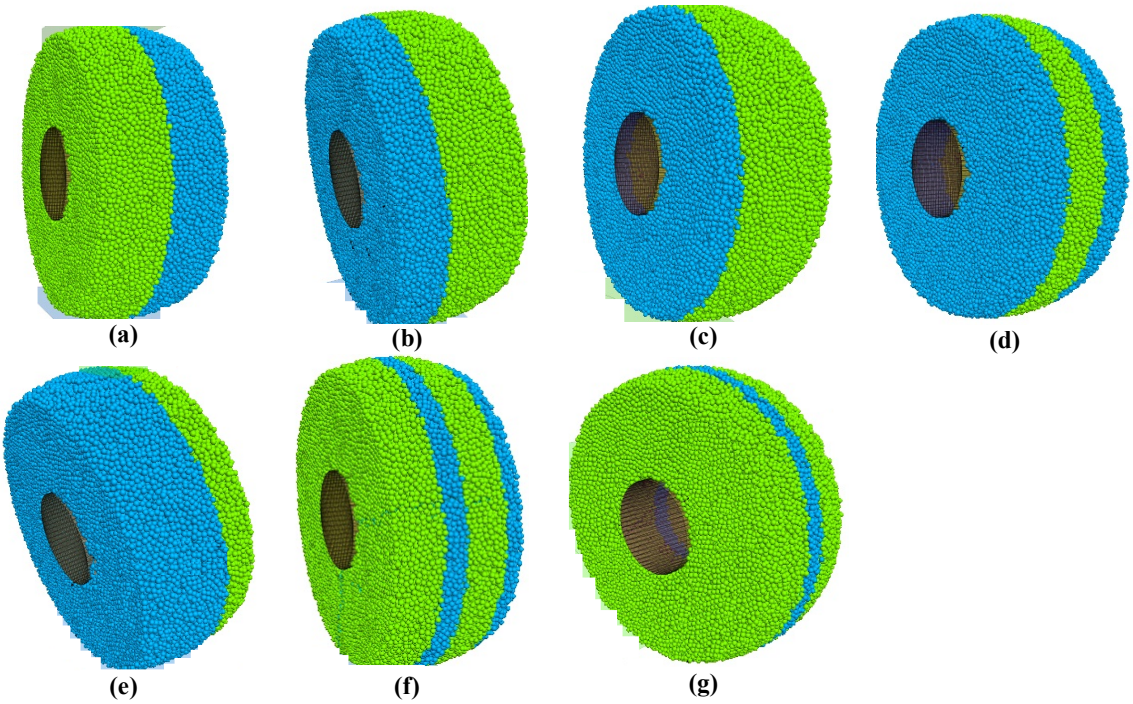

Figure 5. Layered pre-holed models containing two different rocks

3.4. Results of 3D Modeling and Analysis

33.4.1. Tensile Force Generated by Applying Load from Inside the Sample

The tensile force resulting from applying a load within the sample, particularly in the area surrounding the inner cavity (cylinder), is depicted in Figure 6. In the numerical simulation, blue and green lines are utilized to clearly signify the tensile and compressive forces, respectively, exerted on the sample. This figure effectively demonstrates the chain-like arrangement of the tensile force on both sides of the sample within the inner cavity. As the sample experiences higher internal loads, the dimension of the chain-like region transmitting tensile loads around the internal void becomes more distinct.

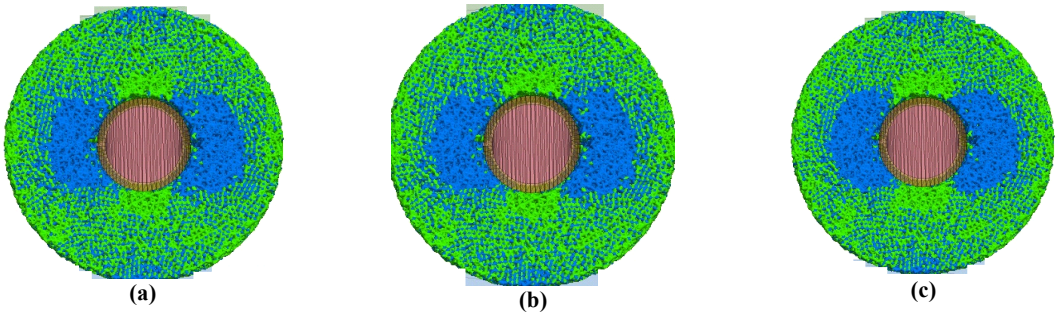

Figure 6 The tensile force resulting from applying a load within the sample, particularly in the area surrounding the inner cavity (cylinder), a) concrete layer percent=77% and gypsum layer percent=23%, b) concrete layer percent=65% and gypsum layer percent=35%, c) concrete layer percent=50% and gypsum layer percent=50%

3.4.2. Direction of Particle Movement in the Anisotropy Model

Figure 7 illustrates the direction of particle movement within the sample, particularly around the inner cavity (cylinder). Movement of particles occurs chiefly along the left and right margins of the central cavity, as depicted in the figure. These movements in these areas suggest that tensile cracking is taking place.

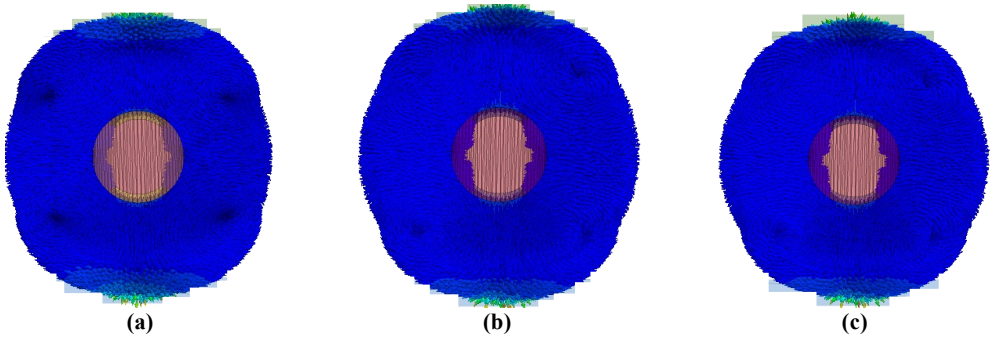

Figure 7. Movement direction of particle around the middle cylinder during internal loading, a) concrete layer percent=77% and gypsum layer percent=23%, b) concrete layer percent=65% and gypsum layer percent=35%, c) concrete layer percent=50% and gypsum layer percent=50%

3.4.3. Stress– displacement behavior in multilayered samples

Figure 8 shows the stress-strain curves for the layered samples with varying layering percentages.

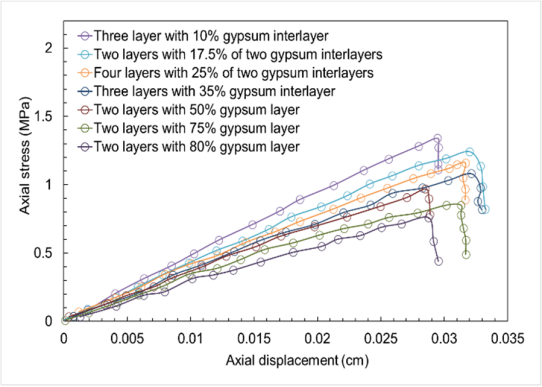

Figure 8. Stress-strain behavior exhibiting linear elasticity up to peak tensile strength for multilayered samples with varying layer percentages

Stress-displacement diagrams effectively illustrate the mechanical behavior (specifically, linear elastic behavior) of bi-material specimens made of gypsum and concrete, up to the peak tensile strength point. Specimens that contain a larger proportion of the rigid concrete layer demonstrate higher tensile strength, suggesting anisotropic properties due to the presence of the weaker gypsum layer. In contrast, the critical strain at maximum tensile load increases when there is a higher proportion of the softer gypsum layer. This means that the failure modes in the layered rock specimens are influenced by the critical strain in the soft layer.

3.4.4. Tensile modulus and concrete layer thickness relations in gypsum-concrete specimens

Figure 9 shows that the tensile modulus, derived from numerical simulations, increases gradually as

the concrete layer thickness increases from 20% to 90% in the modeled gypsum-concrete specimens.

As illustrated in Figure 10, there exists an inverse correlation between the thickness of the gypsum layer and the tensile modulus of the bi-material specimen. This means that, as the gypsum layer becomes thicker, the tensile modulus tends to decrease, and conversely, a thinner gypsum layer corresponds to a higher tensile modulus. The direct physical tests conducted on samples and complementary numerical simulations designed to model the material's behavior have independently corroborated the existence and nature of this inverse relationship.

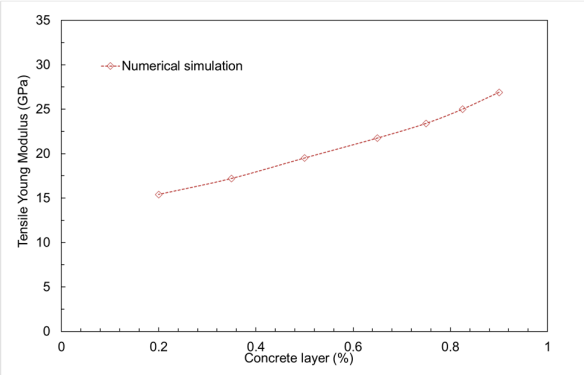

Figure 9. The tensile modulus and concrete layer thickness relations for gypsum-concrete specimens

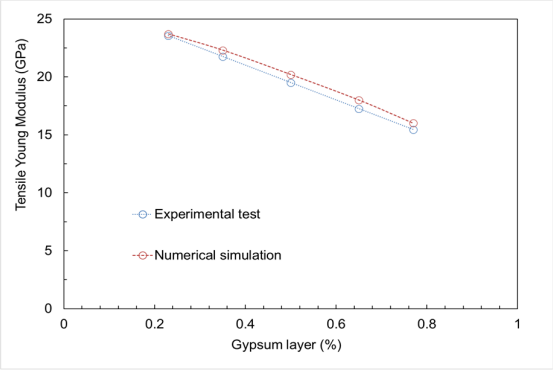

Figure 10. The tensile modulus and gypsum layer thickness relations for bi-material layered rocks

3.4.5. Numerical breakage pattern

The numerical modeling of the failure process and cracking pattern for multilayer specimens containing concrete and gypsum (with specific percentages of each material) is illustrated in Figure 11. In this figure, green represents gypsum while blue represents concrete. It is observed that tensile cracks primarily initiate in the gypsum layer and propagate through the concrete layer in the modeled specimens. Furthermore, Figure 11 depicts the simulated tensile strength under direct tension, showing a strong correlation with the experimental findings presented in Figure 3.

3.4.6. Error Bar Charts and Statistical Analysis

The mean tensile strength, standard deviation, and 95% confidence interval for two-layered specimens with gypsum percentages of 35%, 50%, and 65% are presented in Table 2. The narrow confidence intervals and low standard deviations confirm the high repeatability and statistical reliability of the experimental results. Figure 12 also presents the mean values and error bar charts for the same configurations. The error bars represent the standard deviation of the three repeated tests conducted for each configuration. As observed from Figure 12, the error percentage is within the acceptable range, confirming that the tested specimens exhibited consistent and accurate behavior, validating the effectiveness of the proposed direct tensile testing method for layered specimens.

Table 2. Mean tensile strength, standard deviation, and 95% confidence interval for two-layered specimens with different gypsum percentages.

Gypsum (%)	Mean (MPa)	Std Dev (MPa)	95% CI (MPa)
35	1.100	0.010	(1.075, 1.125)
50	0.900	0.010	(0.875, 0.925)
65	0.800	0.020	(0.750, 0.850)

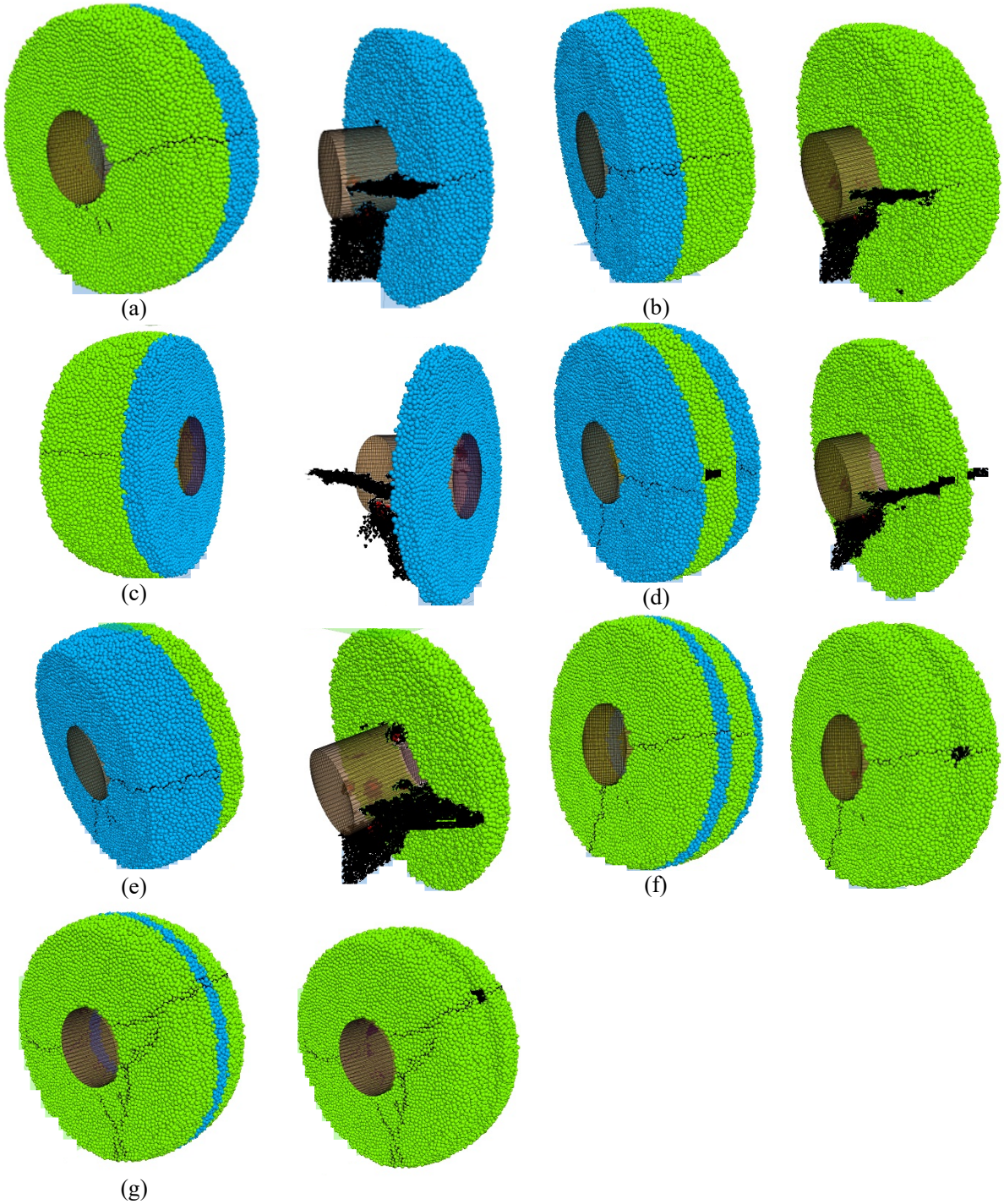

Figure 11. Failure pattern of layered pre-hold ring rock.

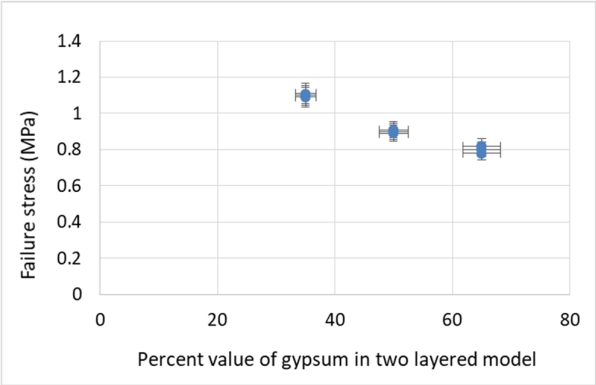

Figure 12. Mean values and error bar charts for two-layered specimens with gypsum percentages of 35%, 50%, and 65%.

4. Conclusions

The findings from the direct tensile tests on layered geo-materials utilizing the novel compressive-to-tensile load-transferring (CTLT) device provide several important insights into the behavior of these materials under stress. The laboratory experiments, supported by three-dimensional particle flow code simulations, revealed that the thickness of the layers plays a significant role in influencing crack propagation paths within the concrete and gypsum layers. Notably, higher percentages of concrete layers correspond to improved tensile strength, while fracture patterns vary depending on the angle of the layers, with angles below 30° resulting in parallel fractures and those above 30° causing interface fractures. Moreover, as the gypsum layer becomes thicker, the observed displacement under maximum load declines, highlighting the complex behavior arising from material interactions in layered constructs. The stress-displacement curves exhibited non-linear characteristics for concrete-dominant models, while gypsum-rich models reflected a linear trend. Furthermore, a reduction in the number of layers was found to enhance tensile strength for a constant material composition, indicating that fewer but thicker layers may be beneficial in optimizing performance. The consistency observed between experimental findings and numerical predictions demonstrates the CTLT device's effectiveness in accurately gauging the tensile strength of brittle layered geo-materials. This novel direct tensile testing method is particularly advantageous as it minimizes complications arising from boundary conditions that typically affect results in alternative testing configurations. As a result, the absence of these boundary effects leads to a more precise evaluation of the material's intrinsic tensile behavior. Furthermore, a strong correlation was identified between tensile strength and the extent of fracturing, with stronger samples exhibiting a greater number of fractures. Altogether, these conclusions reinforce the CTLT device's capability to effectively measure tensile strength and analyze fracture patterns in layered geo-materials.

Statements and Declarations

Data Availability Statement

The data that support the findings of this study are available from the corresponding author upon reasonable request.

Conflict of interest

The authors declare that they have no known competing financial interests or personal relationships that could have appeared to influence the work reported in this paper.

References

[1]. Cho, J., Kim, H., Jeon, S., & Min, K. (2012). Deformation and strength anisotropy of Asan gneiss, Boryeong shale, and Yeoncheon schist. *International Journal of Rock Mechanics and Mining Sciences, 50*, 158–169.

[2]. Bi, J., Du, C., Zhao, Z. Y., Wang, C., Lian, S., & Xiong, X. (2023). Characterization of shear behavior and damage mechanism of periodic thermal loading sandstone based on NMR technique. *Engineering Geology, 325*, 107272.

[3]. Liang, X., Tang, S., Tang, C., Hu, L., & Chen, F. (2023). Influence of water on the mechanical properties and failure behaviors of sandstone under triaxial compression. *Rock Mechanics and Rock Engineering, 56*, 1131–1162.

[4]. Zhao, C., Liu, J., Xu, D., Zhang, L., Lyu, C., & Ren, Y. (2023). Investigation on mechanical properties, AE characteristics, and failure modes of Longmaxi Formation shale in Changning, Sichuan Basin, China. *Rock Mechanics and Rock Engineering, 56*, 1239–1272.

[5]. Fan, W., Zhang, J., Yang, Y., Fang, K., Wu, S., & Xing, Y. (2023). Effects of layering angle and prestress on dynamic load energy conversion and damage mechanism of sandstone. *Processes, 11*(9), 2641.

[6]. Lisjak, A., Tatone, B. S. A., Grasselli, G., & Vietor, T. (2014). Numerical modelling of the anisotropic mechanical behavior of Opalinus Clay at the laboratory-scale using FEM/DEM. *Rock Mechanics and Rock Engineering, 47*, 187–206.

[7]. Heng, S., Guo, Y., Yang, C., Daemen, J. J. K., & Li, Z. (2015). Experimental and theoretical study of the anisotropic properties of shale. *International Journal of Rock Mechanics and Mining Sciences, 74*, 58–68.

[8]. Li, Y., Zhou, H., Zhu, W., Li, S., & Liu, J. (2015). Numerical study on crack propagation in brittle jointed rock mass influenced by fracture water pressure. *Materials, 8*(6), 3364–3376.

[9]. Li, Y., Wang, H., Zhu, W., Li, S., & Liu, J. (2015). Structural stability monitoring of a physical model test on an underground cavern group during deep excavations using FBG sensors. *Sensors, 15*(9), 21696–21709.

[10]. Wang, Y., Li, X., & Zhang, B. (2016). Numerical modeling of variable fluid injection-rate modes on fracturing network evolution in naturally fractured formations. *Energies, 9*(6), 414.

[11]. Wang, Y., Li, X., Hu, R., Ma, C., Zhao, Z., & Zhang, B. (2016). Numerical evaluation and optimization of multiple hydraulically fractured parameters using a flow-stress-damage coupled approach. *Energies, 9*(5), 325.

[12]. Wang, Y., & Li, C. H. (2017). Investigation of the effect of cemented fractures on fracturing network propagation in model block with discrete orthogonal fractures. *Rock Mechanics and Rock Engineering, 50*, 1851–1862.

[13]. Li, Y., Li, C., Zhang, L., Zhu, W., Li, S., & Liu, J. (2017). An experimental investigation on mechanical property and anchorage effect of bolted jointed rock mass. *Geosciences Journal, 21*, 253–265.

[14]. Li, Y., Zhou, H., Dong, Z., Zhu, W., Li, S., & Wang, S. (2018). Numerical investigations on stability evaluation of a jointed rock slope during excavation using an optimized DDARF method. *Geomechanics and Engineering, 14*(3), 271–281.

[15]. Wang, Y., Tan, W. H., Liu, D. Q., Hou, Z. Q., & Li, C. H. (2019). On anisotropic fracture evolution and energy mechanism during marble failure under uniaxial deformation. *Rock Mechanics and Rock Engineering, 52*, 3567–3583.

[16]. Suo, Y., Chen, Z., Rahman, S. S., et al. (2020). Experimental and numerical investigation of the effect of bedding layer orientation on fracture toughness of shale rocks. *Rock Mechanics and Rock Engineering, 53*, 3625–3635.

[17]. Li, K., Yin, Z. Y., Han, D., et al. (2021). Size effect and anisotropy in a transversely isotropic rock under compressive conditions. *Rock Mechanics and Rock Engineering, 54*, 4639–4662.

[18]. Ren, L., Xie, H. P., Sun, X., Zhang, R., Li, C. B., Xie, J., & Zhang, Z. T. (2021). Characterization of anisotropic fracture properties of Silurian Longmaxi shale. *Rock Mechanics and Rock Engineering, 54*, 665–678.

[19]. Golewski, G. L. (2023a). Examination of water absorption of low volume fly ash concrete (LVFAC) under water immersion conditions. *Materials Research Express, 10*(8).

[20]. Golewski, G. L. (2023b). Assessing of water absorption on concrete composites containing fly ash up to 30% in regards to structures completely immersed in water. *Case Studies in Construction Materials, 19*, e02337.

[21]. Golewski, G. L. (2023c). Effect of coarse aggregate grading on mechanical parameters and fracture toughness of limestone concrete. *Infrastructures, 8*(8), 117.

[22]. Golewski, G. L. (2024). Enhancement fracture behavior of sustainable cementitious composites using synergy between fly ash (FA) and nanosilica (NS) in the assessment based on digital image processing procedure. *Theoretical and Applied Fracture Mechanics, 131*, 104442.

[23]. Broch, E. (1983). Estimation of strength anisotropy using the point-load test. *International Journal of Rock Mechanics and Mining Sciences, 20*(4), 181–187.

[24]. Al-Harthi, A. A. (1998). Effect of planar structures on the anisotropy of Ranyah sandstone, Saudi Arabia. *Engineering Geology, 50*, 49–57.

[25]. Wang, G., Yang, D., Liu, S., et al. (2021). Experimental study on the anisotropic mechanical properties of oil shales under real-time high-temperature conditions. *Rock Mechanics and Rock Engineering, 54*, 6565–6583.

[26]. Castro, J., Miranda, M., Olson, M. H., & Justo, J. (2024). Direct tensile testing of Moleanos limestone. *Proceedings of Eurock 2024*, Alicante, Spain.

[27]. Zhang, Y., Zhang, Q.-Y., Zhou, X.-Y., & Xiang, W. (2021). Direct tensile test of red sandstone under different loading rates with the self-developed centering device. *Geotechnical and Geological Engineering, 39*, 709–718.

[28]. Rabat, A., Tomas, R., & Cano, M. (2023). Assessing water-induced changes in tensile behaviour of porous limestones by means of uniaxial direct pull test and indirect methods. *Engineering Geology, 313*, 106962.

[29]. Pérez-Rey, I., Muñoz-Ibañez, A., González-Fernández, M. A., Muñiz-Menéndez, M., Herbón Penabad, M., Estévez-Ventosa, X., Delgado, J., & Alejano, L. R. (2023). Size effects on the tensile strength and fracture toughness of granitic rock in different tests. *Journal of Rock Mechanics and Geotechnical Engineering, 15*, 2179–2192.

[30]. Chenevert, M. E., & Gatlin, C. (1965). Mechanical anisotropies of laminated sedimentary rocks. *Society of Petroleum Engineers Journal, 5*, 67–77.

[31]. Potyondy, D. O. (2017). Simulating perforation damage with a flat-jointed bonded-particle material. *Proceedings of the Fifty First US Rock Mechanics/Geomechanics Symposium*, San Francisco, California, USA.

[32]. Potyondy, D. O., & Cundall, P. A. (2004). A bonded-particle model for rock. *International Journal of Rock Mechanics and Mining Sciences, 41*, 1329–1364.

[33]. Abharian, S., Sarfarazi, V., Rasekh, H., & Behzadinasab, M. (2022). Effects of concrete/gypsum bedding layers and their inclination angles on the tensile failure mechanism: Experimental and numerical studies. *Case Studies in Construction Materials, 17*(1), 89–99.

انجمن مهندسی معدن ایران
نشریه مهندسی معدن و محیط زیست
نشانی نشریه: www.jme.shahroodut.ac.ir
دانشگاه صنعتی شاهرود

توسعه یک روش نوین آزمون کشش مستقیم برای مشخصه‌یابی مواد لایه‌ای: اعتبارسنجی آزمایشگاهی و تحلیل مکانیزم شکست نامتقارن با مدل‌سازی سه‌بعدی PFC

وهاب سرفرازی[۱]، هادی حائری[۲*]، پژمان کلوندی[۱]، علیرضا شاکر[۳]، محمد فاتحی مرجی[۴]، غلامرضا سعیدی[۵]

۱. گروه مهندسی معدن، دانشگاه صنعتی همدان، همدان، ایران
۲. گروه مهندسی معدن، مجتمع آموزش عالی زرند، دانشگاه شهید باهنر کرمان، کرمان، ایران
۳. گروه زمین شناسی، دانشکده علوم، دانشگاه شهید باهنر کرمان، کرمان، ایران
۴. گروه مهندسی استخراج معدن، دانشکده مهندسی معدن و متالورژی، دانشگاه یزد، یزد، ایران
۵. گروه مهندسی معدن، دانشگاه شهید باهنر کرمان، کرمان، ایران

اطلاعات مقاله

تاریخ ارسال: ۲۰۲۶/۰۲/۱۶
تاریخ داوری: ۲۰۲۶/۰۵/۳۰
تاریخ پذیرش: ۲۰۲۶/۰۸/۰۴

DOI: 10.22044/jme.2026.17499.3478

کلمات کلیدی

مدل‌های ناهمسانگردی سه‌بعدی
مقاومت کششی مستقیم
آغازش ترک
نمونه لایه‌ای دارای سوراخ پیش‌ساخته

چکیده

تعیین مقاومت کششی مواد ترد و لایه‌ای، شامل سنگ‌های لایه‌ای و بتن‌های ترک‌دار، هنگام استفاده از آرایش های متداول بارگذاری غیرمستقیم با دشواری‌های قابل‌توجهی همراه است؛ زیرا این روش ها شرایط کشش خالص را در نمونه ایجاد نمی کنند. ازاین‌رو، دستیابی به مقاومت کششی از طریق اندازه گیری مستقیم تجربی، به ویژه در مطالعات مرتبط با آغازش ترک و فرآیند رشد ترک در مجاورت نوک ترک ها، از اهمیت ویژه‌ای برخوردار است. در پژوهش حاضر، یک چارچوب نوین آزمون مبتنی بر کشش مستقیم ارائه شده است که با هدف دستیابی به مشخصه‌سازی دقیق‌تر مقاومت مواد شبه‌ترد لایه‌ای توسعه یافته و به‌طور همزمان امکان بررسی جزئیات مکانیسم‌های آغازش و گسترش شکست را فراهم می‌کند. دستگاه آزمایش پیشنهادی شامل یک تیر فولادی مجهز به مبدل بار است که به‌عنوان مجموعه بارگذاری و همچنین سلول اندازه‌گیری نیرو عمل می‌کند. یک نمونه لایه‌ای دارای سوراخ پیش‌ساخته، به‌صورت ایمن در مرکز دستگاه و به کمک یک صفحه فلزی مقاوم تثبیت شده است. همچنین، کرنش‌سنج‌های نصب‌شده در دو طرف نمونه، داده‌های حیاتی مربوط به رفتار کششی نمونه را ثبت می‌کنند. ویژگی قابل‌توجه این دستگاه، توانایی تشخیص و کمی‌سازی شکست نامتقارن در نمونه است که امکان درک دقیق‌تر الگوهای تشکیل ترک و فرآیند شکست را فراهم می‌سازد. در این تحقیق، طراحی دستگاه، روش‌های کالیبراسیون و نتایج حاصل از آزمون‌های تجربی به‌طور جامع ارائه، بررسی و تحلیل شده‌اند. علاوه بر این، مدل‌سازی سه‌بعدی با استفاده از روش PFC به‌منظور تبیین مکانیسم‌های شکست در آرایش‌های مختلف لایه‌ای انجام شده است که موجب افزایش دقت در اندازه‌گیری مقاومت کششی می‌شود. نتایج مدل‌سازی عددی نشان می‌دهد که با افزایش ضخامت لایه سخت، مقاومت نمونه به‌صورت غیرخطی افزایش می‌یابد. همچنین، در شرایطی که ضخامت لایه سخت ثابت نگه داشته شود، افزایش تعداد لایه‌های سخت موجب کاهش مقاومت مدل می‌شود.

نویسنده مسئول مکاتبات: hadihaeri@uk.ac.ir (ه. حائری)